Dynamic Stability of a Force-Controlled Elastic Robot Manipulator

Mo Shahinpoor and B.C.Chiou[1]

Presented is a simplified dynamic model for a tip force-controlled elastic robot manipulator. Experimental work is then carried out on the dynamic stability of this elastic robot and comparisons are made with the theoretical dynamic simulations. Results show that, during the initial contact process, separation between the manipulator and the environment occurs due to the link elastic motion. This nonlinear effect causes a delay of force actuation and the occurence of impacts, which are significant and detrimental to the system dynamic stability.

INTRODUCTION

For applications such as assembly of mechanical parts or performing machining processes, a robot manipulator is required to interact compliantly with the environment in a prescribed manner [1]. This necessitates the force control at the tip of the manipulator and is often accomplished by means of a wrist force sensor. It is well known that the stability limitation is the major obstacle to achieving a high performance force controller [2-6]. Several possible sources of stability problems have been proposed, which include the link or joint flexibility, actuator bandwidth, drive train backlash, and digital sampling rate.

The force control of robot manipulator using a wrist force sensor is often referred to as a noncolocation control, i.e., the link or joint flexibility exists between the tip force sensor and joint actuator. During the control action, the elastic motion can be excited through dynamic coupling effect. The effect of flexibility on the dynamic stability of force-controlled manipulators has been studied by Chiou and Shahinpoor [7,8]. Assuming the contact point is locked, the link or joint flexibility is explicitly modeled and the compliant equations of motion are derived. The dynamic coupling and unstable behaviors using several force control methods are demonstrated through numerical simulations.

However, due to the assumption that no separation occurs at the contact point, the nonlinear dynamics, such as delay and impact, which occur during the initial contact are excluded. This may not be valid in reality. The purpose of this investigation is to perform the experimental work such that any relevant problems can be identified. For comparison purposes, the discrete-time state-space model for a one-link force-controlled manipulator is derived and numerical simulation is carried out. The experimental results are then presented and comparisons are made with theoretical dynamic simulations.

THEORETICAL MODEL

Figure 1 shows a one-link manipulator which is making contact with the environment. A moving reference frame $\{X_1, Y_1\}$ is attached to the rotating link. The X_1-axis is aligned with the neutral axis of the uniform link. The actuator is a DC motor with an inertia of I_h. The direct-drive

1. Department of Mechanical Engineering, The University of New Mexico, Albuquerque, NM 87131. U.S.A

Scientia Iranica, Vol. 1, No. 1, © Sharif University of Technology, April 1994.

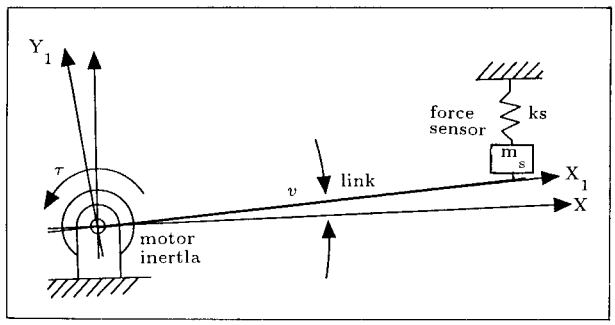

Figure 1. One-link force-controlled manipulator.

flexible link acts as a power transmission device. ℓ is the link length. m_S and k_S are the mass and the stiffness of the force sensor, respectively.

The slender beam is essentially subjected to bending and therefore axial deformation is neglected. The Bernoulli-Euler beam theory is utilized to determine the link elastic deflection. To reduce the degree of freedom of the system, the assumed-mode method is employed to represent the deflection function [9]. That is

$$w(x,t) = \sum_{i=1}^{n} y_i(x)\nu_i(t), \tag{1}$$

where $y_i(x)$ is mode shape function, $\nu_i(t)$ is the modal coordinate (generalized displacement), and n is the number of mode shape functions. The selection of the mode shape functions $y_i(x)$ in Equation 1 requires that the appropriate boundary conditions at the actuator end be considered [10,11]. The pinned-free boundary conditions,

$$\begin{aligned} &w(0,t) = 0,\\ &EIw''(0,t) = -I_h\ddot{w}'(0,t),\\ &w''(\ell,t) = 0,\\ &EIw'''(\ell,t) = m_S\ddot{w}(\ell,t), \end{aligned} \tag{2}$$

are chosen here to solve the mode shape functions. Knowing that the general solution of the eigenfunction is $y(x) = A_1\sin(\beta x)+A_2\cos(\beta x)+A_3\sinh(\beta x)+A_4\cosh(\beta x)$, where $\beta^4 = \omega^2\mu/EI$ and u is the mass per unit length. Here, the normalized eigenfunctions are obtained such that $\int_0^\ell \mu y_i(x)y_i(x)dx = 1$. Note that E is the Young's modulus, I is the area moment of inertia, $(\cdot) = \partial()/\partial t$, and $(') = \partial()/\partial x$ in Equation 2.

The system kinetic energy can be derived as [12]

$$\begin{aligned} T = (a + \sum_{i=1}^{n}\sum_{j=1}^{n}\nu_i\nu_j C_{ij})\dot{\theta}^2 + 2\dot{\theta}(\sum_{i=1}^{n}\dot{\nu}_i E_i)\\ + \sum_{i=1}^{n}\sum_{j=1}^{n}\dot{\nu}_i\dot{\nu}_j C_{ij} + \frac{1}{2}m_S\dot{y}_S^2, \end{aligned} \tag{3}$$

where

$$a = \frac{1}{2}\int_m x^2 dm,$$

$$E_i = \frac{1}{2}\int_m xy_i dm,$$

$$C_{ij} = \frac{1}{2}\int_m y_i y_j dm,$$

$\omega_i = i$th modal frequency of the link,

$\dot{\theta}$ = joint velocity.

Assuming the contact point is locked, the potential energy is given as

$$P = \sum_{i=1}^{n}\frac{1}{2}\nu_i^2\omega_i^2 + \frac{1}{2}k_s y_s^2, \tag{4}$$

where ω_i is the ith modal frequency.

Given the expressions for kinetic and potential energy and the displacement constraint at the tip

$$y_s = \ell\theta + \sum_{i=1}^{n}\nu_i y_i(\ell), \tag{5}$$

the equations of motion are derived using the Lagrange's principle in conjunction with the Lagrange multipliers. It may be shown that

$$M\ddot{z} + Kz = F, \tag{6}$$

where

$$M = \begin{bmatrix} 2a + I_h + m_s\ell^2 & 2E_1 + m_s\ell y_1 & 2E_2 + m_s\ell y_2 \\ 2E_1 + m_s\ell y_1 & 2C_{11} + m_s y_1^2 & 2C_{12} + m_s y_1 y_2 \\ 2E_2 + m_s\ell y_2 & 2C_{21} + m_s y_1 y_2 & 2C_{22} + m_s y_2^2 \end{bmatrix}$$

$$K = \begin{bmatrix} k_s\ell^2 & k_s\ell y_1 & k_s\ell y_2 \\ k_s\ell y_1 & k_s y_1^2 + \omega_1^2 & k_s y_1 y_2 \\ k_s\ell y_2 & k_s y_2 y_1 & k_s y_2^2 + \omega_2^2 \end{bmatrix},$$

$z = (\theta, \nu_2, \nu_2)^T$,

$F = (\tau, 0, 0)^T$,

$y_i = y_i(\ell)$,

$\tau =$ joint torque.

Note that the higher-order nonlinear terms are ignored and only the first two mode shape functions ($n = 2$) are considered. Also, the assumption that the contact point is locked is employed to simplify the model. In other words, any possible occurrence of the separation, and thus the impact, during the compliant motion is excluded and ignored. Therefore, Equation 6 is valid only under the constraint that the continuous contact between the sensor and the environment is always present.

Since digital control is used for the experiment, a discrete-time state-space representation of Equation 6 is required. To achieve this, Equation 6 is converted to its state-space form first such that

$$\dot{x} = Fx + Gu,$$
$$y = Hx, \tag{7}$$

where

$x = (\theta, \nu_1, \nu_2, \dot{\theta}, \dot{\nu}_1, \dot{\nu}_2)^T$

$$F = \begin{bmatrix} 0 & I \\ -M^{-1}K & 0 \end{bmatrix},$$

$u = \tau$,

$G = (0, 0, 0, M_{11}^{-1}, M_{21}^{-1}, M_{31}^{-1})^T$,

$H = (k_s\ell, k_s y_1, k_s y_2, 0, 0, 0)$,

$y =$ the contact force.

Having written Equation 7, the discrete-time state-space equations can be derived accordingly [13],

$$x_{k+1} = \Phi x_k + \Gamma u_k,$$
$$y_k = H x_k, \tag{8}$$

where

$$\Phi = e^{FT} dt,$$

$$\Gamma = \int_0^T e^{F\eta} d\eta G,$$

$T =$ sampling period.

The purpose of this investigation is to explore the stability limitation due to the link flexibility. Therefore, a simple explicit force control is selected to suit this purpose [Whitney, 1979], namely,

$$\tau = K_f(f_c - f_d) - K_v\dot{\theta} + \ell f_d, \tag{9}$$

where K_f is the proportional gain, f_c is measured contact force, f_d is the desired contact force, K_v is the derivative gain, and ℓf_d is the feedforward torque. Note that, if the link is rigid, the servo damping term, $-K_v\dot{\theta}$, can be thought of as a damping to the contact force since $\dot{f}_c = k_s\ell\dot{\theta}$.

A slender aluminum beam is selected for the numerical simulation and experimentation. The physical parameters and modal analysis data are shown in Tables 1 and 2. The computed numerical values for Φ, Γ, and H are listed in appendix B. Given the control gains, the simulation results obtained by using Equations 8 and 9 are shown in Figure 2. The force trajectories with different values of K_f and fixed

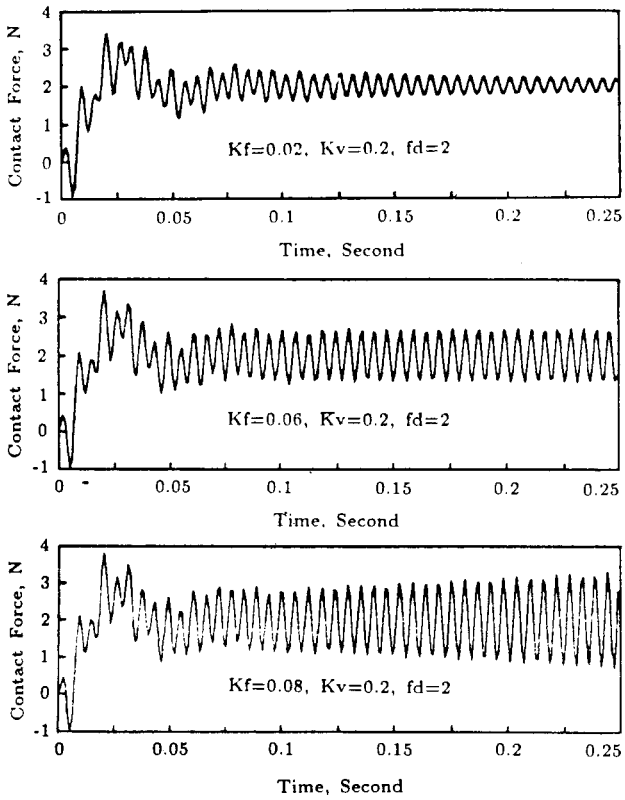

Figure 2. Numerical simulation results.

values of K_v and f_d are plotted. With $K_f = 0.08$, the growing pattern of the force trajectory indicates an unstable behavior due to the link flexibility [7]. Note that the initial negative (tension) force is due to the assumption that the contact point is locked. This implies that separation between the link and sensor might occur in real situations.

Table 1. Physical Parameters

link length=0.454 m
cross section: 3.17 mm× 12.7 mm
link mass=0.0484 kg
motor inertia=1.2×10^{-3} kg-m^2
$m_s = 8.29 \times 10^{-4}$ kg
$k_s = 7.12$ N/mm

EXPERIMENTAL APPARATUS

A schematic of the experimental setup for the one-link flexible manipulator is shown in Figure 3. The major components include a DC motor, a pulse-width modulation amplifier, a slender aluminum beam, and a force sensor. The motor is a high-torque DC motor with peak stall torque of 7.5 Nm and an inertia of 1.2×10^{-3}kg$-$m^2. The controller consists of an IBM-AT personal computer and two interface boards (timer, A/D and D/A converters). Figure 4 shows the control block diagram.

The setup was as follows:

$K_D = 2.44E - 3$ V/count,
$K_A = 2.807$ A/V,
$K_I = 0.23$ Nm/A,
$K_F = 0.2787$ V/N,
$K_T = 0.091$ V-sec/rad,
$K_C = 409.6$ count/V,
T = sampling period = 1 ms.

The force sensor is made of a 2 in cantilever beam with two strain gauges mounted

Table 2. Modal Analysis Data

$\omega_1^2 = 2.213 \times 10^4$ rad^2/sec^2
$\omega_2^2 = 2.684 \times 10^5$ rad^2/sec^2
$y_1(\ell) = -11.011$ m
$y_2(\ell) = 9.168$ m
$a = 0.1663 \times 10^{-2}$ kg-m^2
$E_1 = -2.367 \times 10^{-2}$ kg-m^2
$E_2 = -4.798 \times 10^{-3}$ kg-m^2
$C_{11} = 0.5$ kg-m^2
$C_{12} = C_{21} = -0.188$ kg-m^2
$C_{22} = 0.5$ kg-m^2

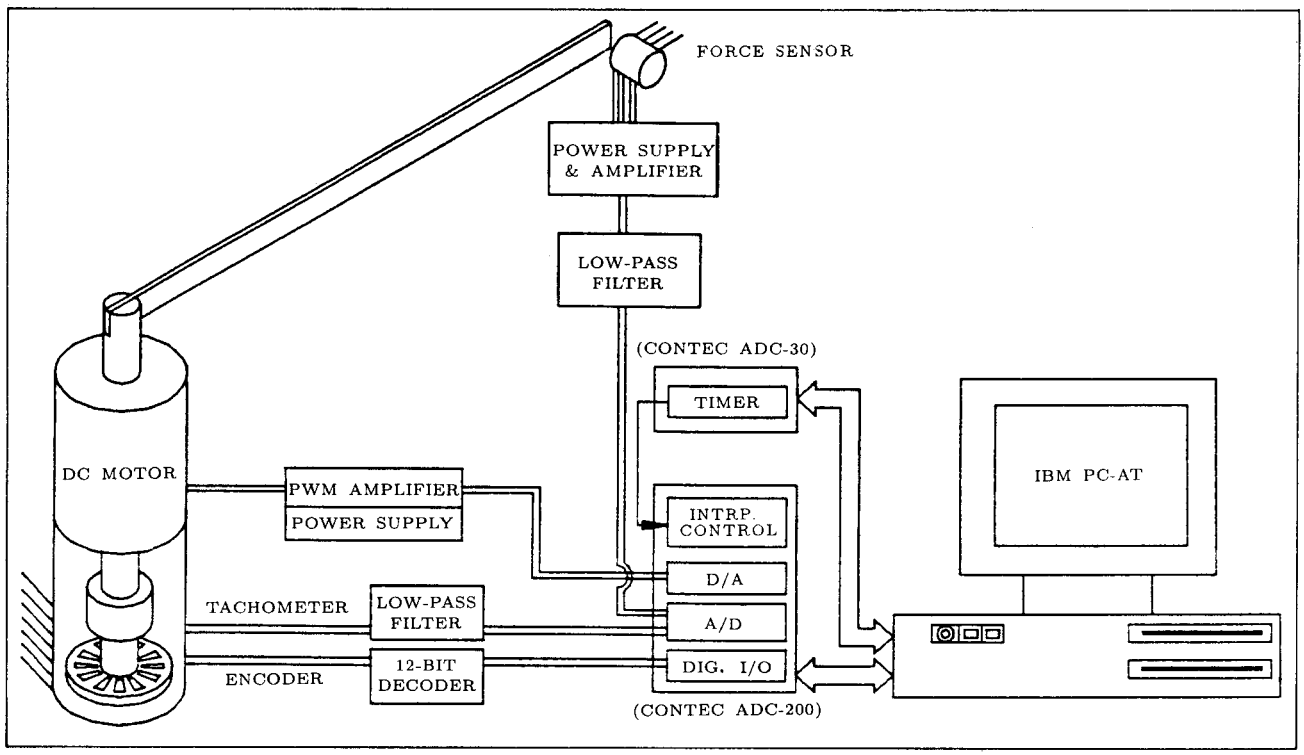

Figure 3. Experimental setup.

on each side (see Figure 5). For each gauge, $w = 1/16$n (1.587 mm) and $h = 1/2$ in (12.7 mm). The contact between the flexible link and the force sensor in achieved by using a small set screw which is tightly mounted at the tip of the link. The diameter of the contact area is 2 mm. The strain signal from the force sensor is amplified 15 times and sent to a low-pass filter with a cutoff frequency of 1600 Hz.

EXPERIMENTAL RESULTS

The selection of the appropriate boundary conditions for a rotating flexible link with an actuator inertia at its end has long been a controversial issue [10,11]. The result of a random excitation

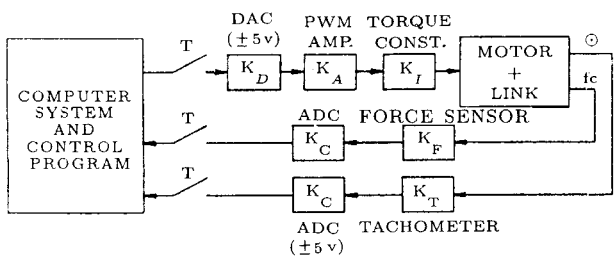

Figure 4. Control block diagram.

test for the free motion case is presented here to clarify this ambiguity [12]. (Although this investigation is focused on the compliant motion of a flexible link, the same boundary conditions with the free motion case are applied at the actuator end). The experimental beam is made of a 24-inch aluminum beam with $1/2'' \times 1/16''$ cross section, which is a different set up from what is described in Table 1. The strain gauges are mounted on the link near the actuator end. The actuator is a Galil 50/1000 DC motor with inertia of 2.6×10^{-5} kg-m^2. The random excitation is performed by sending a white-noise torque command with 100–Hz flat range to the motor and the the strain signal is recorded. Figure 6 shows the power spectral density (PSD) function of the strain signal. The spikes denote the natural frequencies which closely match with the computed values using Equation 2.

As regards the compliant motion tests, the physical parameters for the motor and link assembly are listed in Table 1. Note that a lumped-mass model considering only the first mode of a cantilever beam is used to represent

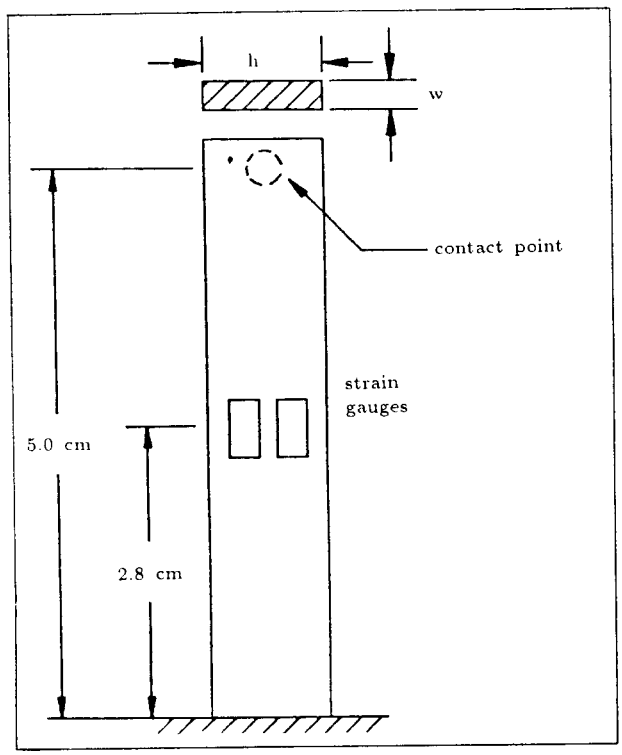

Figure 5. Force sensor.

the sensor dynamics. The computed values of mass and stiffness are m_s and k_s, respectively.

Figure 7 shows the open-loop test results with a step torque command $\tau = 1$ Nm. Note that the link is manually moved to make an initial contact with the force sensor to minimize the impact effect. Then, the torque command is triggered. The initial slow variation of the force trajectory is due to the rigid body motion of the motor, which is evidenced by the similar,

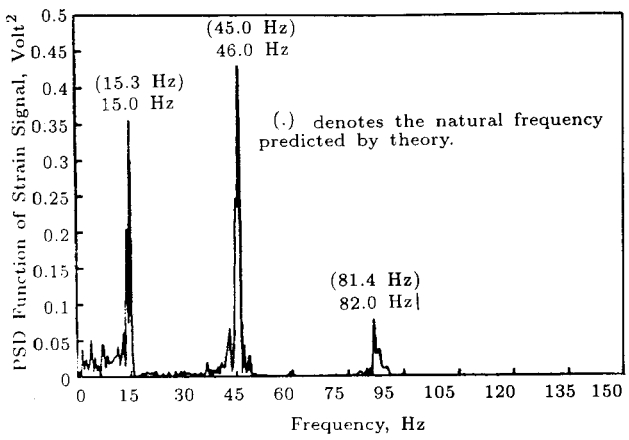

Figure 6. PSD function of strain signal.

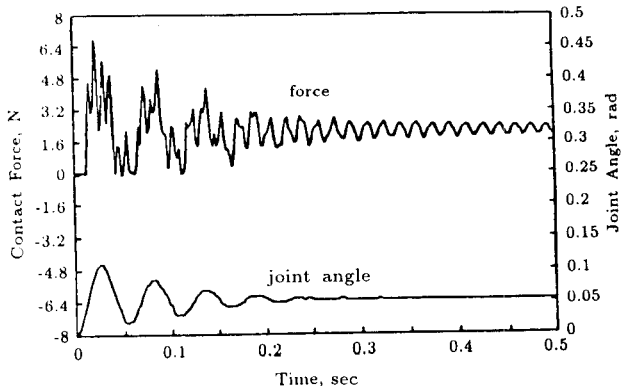

Figure 7. Open-loop step response.

pattern of joint angle trajectory. Due to the link flexibility, the force trajectory exhibits some oscillations on top of the slow variation, which gradually die out because of the structural damping and the joint static friction, which is above 0.07 Nm.

As shown in Figure 7, the force trajectory also indicates a 'time delay' between the motor torque and the output of the force sensor, i.e., $f_c = 0$ and $\theta \neq 0$ for $t = 0$ to 0.012 second. To examine this time lag phenomenon, a numerical simulation of the tip position due to a unit step torque is carried out. Note that the equations of free motion (shown in Appendix A) are used for this purpose since no compliant force is in action yet. Figure 8 shows the result. The tip position appears to be quasi-stationary during the first 10 ms. This is because of the fact that while the link is moving in the motor torque direction, the tip is moving in the opposite direction due to the link elastic motion [10]. Considering that the contact force results from the overall tip displacement, this explains the time delay behavior.

The following sections present the closed-loop test results using the explicit force control law, Equation 9. Figure 9 shows the effect of the proportional gain and $K_f = 0.04$ is approximately the critical gain. The time delay behavior shows up in each of the force trajectories. The limit cycle behavior is exhibited with $K_f = 0.04$. Several observations can be made by comparisons to the similar cases shown in Figure 2. The major difference here is that the contact point

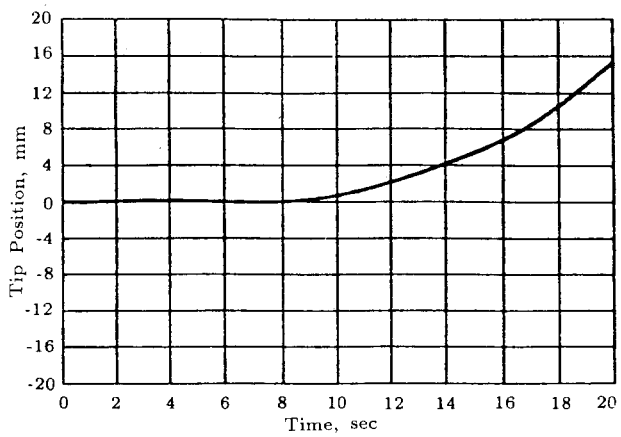

Figure 8. Step response of tip position.

is free rather than locked to the sensor. Right after the motor torque is triggered, the loss of contact occurs due to the link elastic motion. The transient part of force response does not appear. Instead, the force trajectory is characterized by a delay and then an oscillation with impact-like response. In other words, due to the nonlinear effects of delay and impacts, the system actually becomes more unstable. Figure 10 shows the results with different values of reference commands. Although the proportional gain is less than the critical value, the system is unstable when the force command is small (see Figure 10a). This indicates another effect of impact and it will dominate the system dynamics if the reference command is small [14,15].

To avoid the loss of contact, an open-and-then-closed-loop control is devised. The experiment is conducted by first commanding a static torque of 0.5 Nm for 2 seconds and then switching to the closed-loop control. Figure 11a shows the test result corresponding to the closed-loop control. The sharp drop of the contact force is compensated by the initial nonzero force such that the continuous contact ($f_c > 0$) is retained. The result of numerical simulation using nonzero initial conditions is shown in Figure 11b. Comparison indicates that a reasonable agreement is obtained, although the analytical model is somewhat more stiff than the real system. This suggests that the open-loop control can minimize the impact effect and improve the system stability.

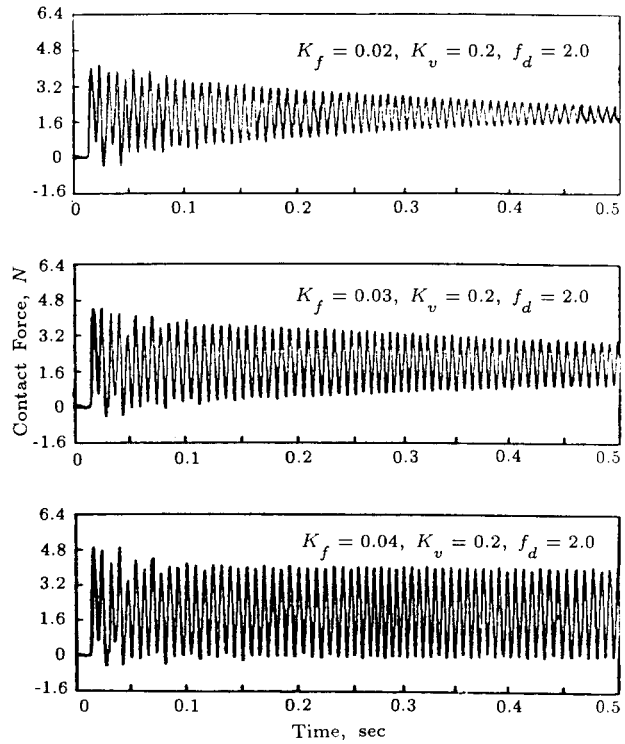

Figure 9. Effect of proportional gain.

CONCLUSIONS

The governing equation of a one-link flexible manipulator is dynamically simulated assuming no separation at the contact point for force control. This model shows that the elastic modes can be excited by force control action, which can in turn make the system unstable. However, experimental results indicate other significant and detrimental effects due to the link flexibility,

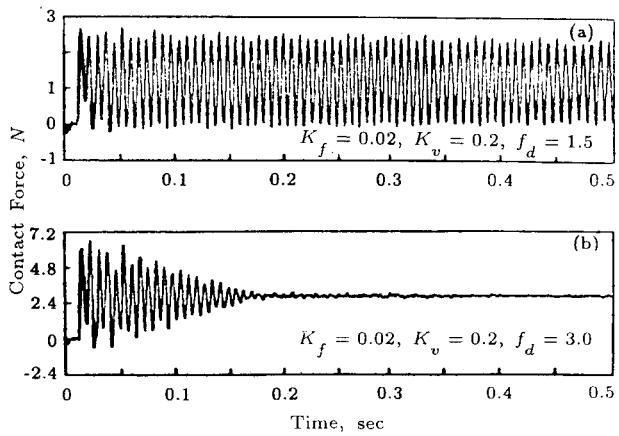

Figure 10. Effect of different reference force commands.

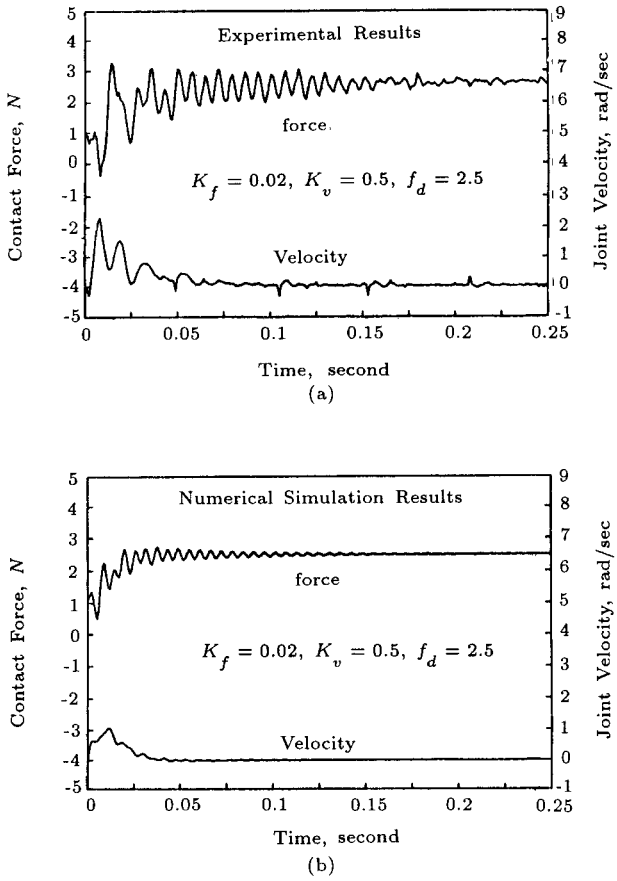

Figure 11. Results of open-and-closed-loop control.

namely, delay and impact. These highly nonlinear phenomena are experimentally evidenced by the dependence of system stability on the reference input and the initial conditions. The open-and-closed-loop test indicates that these nonlinear effects can be minimized by preloading an initial contact force through open-loop control.

REFERENCES

1. Whitney, D.E. "Historical perspective and state-of-the-art in robot force control," *Proc., IEEE Int. Conf. on Robotics and Automation* (1985).
2. An, C.H. and Hollerbach, J.M. "Dynamic stability issues in force control of manipulators," *Proc., IEEE Int. Conf. on Robotics and Automation* (1987).
3. An, C.H. and Hollerbach, J.M. "Kinematic stability issues in force control of manipulators," *Proc., IEEE Int. Conf. on Robotics and Automation* (1987).
4. Eppinger, S.D. and Seering, W.P. "On dynamic models of robot force control," *Proc., IEEE Int. Conf. on Robotics and Automation* (1986).
5. Eppinger, S.D. and Seering, W.P. "Understanding bandwidth limitations in robot force control," *Proc., IEEE Int. Conf . on Robotics and Automation* (1987).
6. Eppinger, S.D. and Seering, W.P. "Three dynamic problems in robot force control," *Proc., IEEE Int. Conf. on Robotics and Automation* (1989).
7. Chiou, B.C. and Shahinpoor, M. "The effect of joint flexibility on the dynamic stability of a one-link force-controlled manipulator," *Robotica International Journal,* **7**, pp 339-342 (1989).
8. Chiou, B.C. and Shahinpoor, M. "The effects of joint and link flexibilities on the dynamic stability of force-controlled manipulators," *Proc., IEEE Int. Conf. on Robotics and Automation,* pp 398-403 (1989).
9. Meirovitch, L. *Analytical Methods in Vibrations,* The Macmillan Company, London (1967).
10. Schmitz, E. "Experiments on the end-point position control of a very flexible one-link manipulator," PhD thesis, Stanford University, Stanford, CA, USA (April 1985).
11. Barbieri, E. and Özguner, Ü. "Unconstrained and constrained mode expansions for a flexible slewing link," *ASME J. of Dynamic Systems, Measurements and Control,* **110**, pp 416-421 (1988).
12. Chiou, B.C. "Theoretical and experimental investigations of dynamics and stability of flexible manipulators," PhD thesis,

University of New Mexico, USA (May 1990).

13. Franklin, G.F. and Powell, J.D. *Digital Control of Dynamic Systems,* Addison Wesley, Reading, MA (1980).
14. Youcef-Toumi, K. and Gutz, D.A. "Impact and force control," *Proc., IEEE Int. Conf. on Robotics and Automation* (1989).
15. Chiou, B.C. and Shahinpoor, M. "Experimental and theoretical observations on the dynamic stability of a one-link force-controlled flexible manipulator," *Proc, IEEE Int. Conf. on Robotics and Automation,* pp 1208-1213 (1991).

Appendix A

Equations of motion moving in free space:

$$\begin{bmatrix} 2a+I_h & 2E_1 & 2E_2 \\ 2E_1 & 2C_{11} & 2C_{12} \\ 2E_2 & 2C_{21} & 2C_{22} \end{bmatrix} \begin{Bmatrix} \ddot{\theta} \\ \ddot{\nu}_1 \\ \ddot{\nu}_2 \end{Bmatrix} + \begin{bmatrix} 0 & 0 & 0 \\ 0 & \omega_1^2 & 0 \\ 0 & 0 & \omega_2^2 \end{bmatrix} \begin{Bmatrix} \theta \\ \nu_1 \\ \nu_2 \end{Bmatrix} = \begin{Bmatrix} \tau \\ 0 \\ 0 \end{Bmatrix}, \tag{A-1}$$

Tip displacement:

$$d_{tip}(t) = \ell\theta(t) + y_1(\ell)\nu_1(t) + y_2(\ell)\nu_2(t) \tag{A-2}$$

Appendix B

$$\Phi = \begin{bmatrix} 9.178e-1 & 1.535e+0 & -4.472e+0 & 9.710e-4 & 5.494e-4 & -1.545e-3 \\ 6.826e-3 & 7.953e-1 & -9.579e-!2 & 2.297e-6 & 9.310e-4 & -3.268e-5 \\ -1.406e+2 & 2.518e+3 & -8.136e+3 & 9.178e-1 & 1.535e+0 & -4.472e+0 \\ 1.332e+1 & -3.990e+2 & -1.804e+2 & 6.826e-3 & 7.953e-1 & -9.579e-2 \\ -1.757e+1 & 3.892e+2 & -7.916e+2 & -1.006e-2 & 2.247e-1 & 5.644e-1 \end{bmatrix}, \tag{B-1}$$

$$\Gamma = (3.448e-4 \;\; 2.063e-5 \;\; 1.048e-5 \;\; 6.740e-1 \;\; 4.027e-2 \;\; 1.973-2)^T, \tag{B-2}$$

$$II = (3.232e+3 \;\; -7.839e+4 \;\; 6.527e+4 \;\; 0 \;\; 0 \;\; 0) \tag{B-3}$$